Journal of Materials Chemistry C

Accepted Manuscript

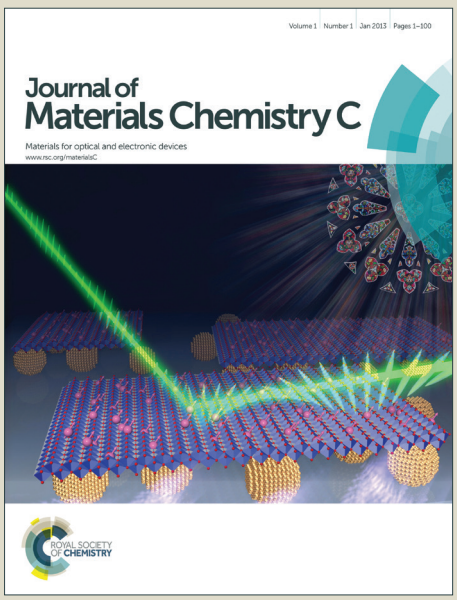

ROYAL SOCIETY OF CHEMISTRY

www.rsc.org/materialsC

Journal Name

RSCPublishing

ARTICLE

Water dispersible electrically conductive poly (3,4-ethylenedioxythiophene) nanospindles by liquid crystalline template assisted polymerization.

Sudha J. Devaki[a*], Neethu K. Sadanandhan[a], Renjith Sasi[a], Hans-Juergen P. Adler[c] , Andrij Pich[b*]

Cite this: DOI: 10.1039/xoxxoooooox

Received ooth January 2012,
Accepted ooth January 2012

DOI: 10.1039/xoxxo

www.rsc.org/

[a]*Chemical Sciences and Technology Division, National Institute for Interdisciplinary Science and Technology (NIIST), CSIR, Thiruvananthapuram 695 019, India.*

[b] *Leibniz Institute of Interactive Materials, Functional and Interactive Polymers, RWTH Aachen University, D-52056 Aachen, Germany.*

[c]*Department of Macromolecular Chemistry and Textile Chemistry, University of Technology, Dresden, Germany*.

In this work, we demonstrate a inimitable liquid crystalline template strategy for the preparation of water dispersible electrically conducting poly(3,4-ethylenedioxythiophene) nanospindles (PEDOTS). PEDOTSs were formed during the polymerization of spindle shaped liquid crystalline phase of "EDOT-PDPSA" which was formed by the specific interactions of 3, 4-ethylenedioxythiophene (EDOT) with 3-pentadecyl phenol-4-sulphonic acid (PDPSA). Liquid crystalline phases were characterized by Polarized Light Microscopic (PLM) analyses, rheology and XRD. Morphology and solid state ordering of conducting nanospindles were characterized by SEM, TEM and XRD. PEDOTS nanospindles exhibited an electrical conductivity of ~2.79 S/cm and good thermal stability (~300 ˚C), which suggests its applicability in fabricating high temperature electronic devices. Furthermore, electrochemical studies of PEDOTS modified glassy carbon electrode (GCE) showed oxidation peak of ascorbic acid at a lower potential of 0.046 V with peak current about 10 times (91.68 µ A) higher than that of the bare GCE with excellent electrode stability, proposes that it can be used as a steady electrode for the electro-catalytic oxidation of similar molecules.

1 Introduction

Nanostructured intrinsically conducting polymers (ICP)s have attracted tremendous attention in the past decade due to their extended π- conjugated chains, reversible doping and dedoping capability, good electrical conductivity and tunable electrochemical behaviours.[1] They have been used for fabricating organic light weight batteries, antistatic coatings, EMI shieldings, flexible photovoltaics, efficient sensors and memory devices.[2-4] However, development of nanoscopic conducting polymers with pointed ends such as nanospindles are receiving enormous interest as it can facilitate the smooth transfer of charge carriers from end to end. Among the various ICPs, poly (3,4-ethylenedioxythiophene) (PEDOT) has been identified as a reliable functional material for a wide range of applications because of its optical transparency, low band gap, flexibility, ease of preparation, thermal stability, versatility for side chain functionalization and bioconjugation.[5-11] These properties makes ICPs based on PEDOTS an unavoidable part in flexible organic photovoltaics.

Due to the scientific urge in creating ecofriendly materials in the nanoscopic regime for energy harvesting, there is remarkable research interest in the area of water dispersible PEDOT nanostructures.[12] In combination with polyelectrolytes such as poly(styrenesulfonate) PEDOT forms water dispersible highly conducting transparent films which has been utilized in

solar devices as a hole transport layer.[13] Several promising strategies based on self assembly were reported for the preparation of nanoscale PEDOT materials by the manoeuvring of non-covalent interactions such as hydrogen bonding, van der Waals forces, π - π stacking and so forth.[14] Major synthetic strategies involve conducting chemical or electrochemical template guided polymerisation. Templates can be micelles or liquid crystalline phases of anionic, cationic or non-ionic surfactants in aqueous solutions with concentrations greater than critical micelle concentration (CMC).[15-19] Self assembled surfactant molecules in specific mesophases can serve as the templates during polymerization. The well-ordered channels present in the mesophase could be utilized as structure-directing strategy for tuning the size and shape of the targeted functional nano materials. Recently, Stup et al. utilized lyotropic hexagonal mesophase as template for the electrochemical polymerization of PEDOT, which could imitate the texture and birefringence of the LC template.[20] A. Pich et al. reported the use of microgel particles as microreactors for the deposition of functional conducting polymers.[21] H. Mao et al. synthesized nanospindles of β-akaganeite containing PEDOT using $FeCl_3.6H_2O$ as an oxidant initiator in aqueous solution in presence of template formed by cetyl trimethyl ammonium bromide and poly(acrylic acid).[22]
Recently petroleum based surfactants becomes expensive due to their increased demand and depletion of resources. So researchers are looking for renewable resource based low cost and abundantly available molecules for their research. Among these cashew nut shell liquid (CNSL) can be considered as an alternate source for unsaturated long chain phenols. It is a low cost, abundantly available industrial byproduct obtained from the cashew industry. The main constituent of CNSL is cardanol (3-pentadecyl phenol), which can be separated by distillation process. 3-pentadecyl phenol-4-sulphonic acid, denoted as PDPSA is a sulphonic acid derivative of cardanol. It has a unique built-in amphiphilic design consisting of hydrophilic sulfonic acid head group and a hydrophobic tail made up of 15 carbon long alkyl chain. Development of nanostructured conducting polymer-clay nanocomposite using PDPSA as structure directing agent cum intercalating agent was earlier reported from our group.[23-24] In the present work, the unique amphiphilic nature of the EDOT-PDPSA adduct is utilized for the generation of thermodynamically stable self-organized lyotropic liquid crystalline template both in water and water-ethanol media. Liquid crystalline phase formation of EDOT-PDPSA was studied by polarised light microscopy, rheology and XRD. Later, EDOT-PDPSA in its liquid crystalline phase was polymerized to form PEDOTS nanospindles. Effects of temperature, solvent and reaction time on the molecular weight, electrical conductivity, morphology and crystalline order were studied. Then glassy carbon electrode was modified with PEDOTS nanospindles and studied its efficiency in the electrocatalytic oxidation of Ascorbic acid.

2 Experimental

2.1 Materials and methods

3-Pentadecylphenol-4-sulfonic acid was prepared from 3-pentadecyl phenol as per the reported procedure (ESI).[25] 3,4-ethylenedioxythiophene and ferric chloride hexahydrate were purchased from Aldrich and used as such. All solutions were prepared in doubly distilled water.

2.2 Preparation and characterisation of liquid crystalline template, EDOT–PDPSA.

Lyotropic liquid crystalline behavior of EDOT-PDPSA was studied both in water and ethanol-water mixture (3:7). Critical micelle concentration (CMC) and liquid crystalline phase formations were studied by adjusting the amount of the EDOT-PDPSA both in water and ethanol-water mixture. CMC was evaluated by conducting UV-Vis absorption measurements of solutions with varying concentrations. The concentration corresponding to the inflection point in the absorbance vs. concentration plot was taken as the CMC. Typical curve is given in the supporting information (Fig. S1). Concentration of EDOT-PDPSA was further increased both in water and water-ethanol media to observe liquid crystalline phases under PLM and was confirmed by rheological analyses using the same solutions.
Typical procedure for the preparation of LC template is given below.
0.5g of PDPSA(1.3×10^{-4} mole) was mixed with 0.02g of EDOT(1.3×10^{-4} mole) and then dispersed in 10 mL of doubly distilled water with heating and stirring for 1 h at 60-70°C.

2.3 Synthesis of PEDOT-PDPSA

Polymeriation experiments were performed in liquid crystalline phase of the self-organized "EDOT-PDPSA" using oxidative intiator ferric chloride hexahydrate. Experiments were performed both in water and ethanol-water mixture (3:7) at 20 and 60 °C. Typical procedure: 0.52 g of EDOT-PDPSA (1.3×10^{-4} mole) in LC phase was taken in 25 mL three necked round bottomed flask provided with a magnetic stirrer. To this solution, ferric chloride hexahydrate (0.23g) (1.3×10^{-4} mole) was added dropwise with stirring at 20 °C. As time passes the resultant solution changed its color from orange red to brown and then to green. Reaction was allowed to continue for 24 hrs. Then residue was collected under centrifugation using an ultra-centrifuging apparatus operating at 20,000 rpm for 20 minutes at 20 °C. Filtrate was removed using a dropper and again redispersed in water using a ultrasonicator. Washing and centrifugation repeated several times for the complete removal of the byproducts and the unreacted oxidants until the filtrate become colourless. The solid product was dried in a vacuum oven at 60 °C for 24 hrs. Experiments were also performed using EDOT without template. PEDOTs prepared under different conditions were designated as PEDOTS1 (ethanol-water at 20 °C), PEDOTS2 (ethanol-water at 60 °C), PEDOTS3

(water at 20 °C), PEDOTS4 (water at 60 °C) and PEDOT (control sample prepared without template).

2.4 Fabrication of PEDOTS modified GCE for electrochemical analysis.

Aqueous dispersion of PEDOTS (2.5 mg/mL) was prepared and dropped on the surface of a pre-cleaned GCE and kept under vacuum for the evaporation of water to form a uniform film over the GCE. This modified GCE was used as the working electrode for studying the electrocatalytic activity during the oxidation of ascorbic acid.

2.5 Instrumentation

UV-Vis absorption spectra were studied using UV-Vis spectrophotometer [Shimadzu model 2100, Japan] in the range of 300-1100 nm. FT-IR spectral measurements were made using fully computerized Nicolet impact 400D FT-IR spectrophotometer (Czech Republic, EU). X-ray diffraction studies were done using powder X-ray diffractometer (Philips X'pert Pro, Netherlands) with CuKα radiation (λ~0.154 nm) employing X'celarator detector and monochromator at the diffraction beam side. Thin films casted on glass plates were used employing standard sample holder. Electrical conductivity (σ_{dc}) of pellets were measured using the standard spring loaded pressure contact four- probe method using a Keithley 6881 programmable current source and 2128A nano-voltmeter at 30° C supplied by Keithley (Germany) as per the standard procedure ASTM F 43-99. For conductivity measurements, the samples were pressed into 5 mm diameter disk using hydraulic press operated at a pressure of 200 MPa. The conductivities of the samples were measured at three different positions, and at least three pellets were measured for each sample: an average of nine readings was used for conductivity calculations. Polarised light micrographs (PLM) were taken in an Olympus BX 51 microscope after drop casting the solution of sample in a clean dry glass plate. For SEM measurements, samples were subjected for thin gold coating using a JEOL JFC-1200 fine coater. The probing side was inserted into JEOL JSM- 5600 LV scanning electron microscope for taking photographs. Transmission electron microscopy was performed in a FEI, TEC NAI 30G2 S-TWIN microscope with an accelerating voltage of 100 KV. For TEM measurements, the water suspensions of samples were fully dispersed under ultrasonication. Then deposited on formvar coated copper grid and dried at room temperature before observation. Rheological property of various phases was measured using Anton Paar Modulated Compact Rheometre-150 Physica (Germany). Parallel plate sensor with a diameter of 50 mm and a gap size of 0.25 mm were used and measurements were done in dynamic oscillatory mode. Thermal stability measurements were performed at a heating rate of 10 °C/min in nitrogen atmosphere using Schimadzu, DTG–60 equipment. Molecular weight was measured using MALDI TOF mass spectrometer (AXIMA CFR, Shimadzu) equipped with a nitrogen laser emitting at 337 nm and α-cyano-4-hydroxy cinnamic acid as the matrix. All cyclic voltammetry studies were performed in an Electrochemical CH Analyser. Experiments were done at ambient temperature in a one-compartment electrochemical cell with a three electrode system. Saturated Ag/AgCl electrode was used as the reference electrode and platinum wire with 0.5 mm diameter and 50 mm length were used as the auxiliary electrode. All the experiments were carried out at 25 ± 5^0C. Before performing the experiments, the solution was purged with nitrogen gas for 10 minutes and current was passed.

3 Results and discussion

3.1. Structure and properties of EDOT–PDPSA

The stability and formation of adduct was theoretically confirmed by energy minimization using Gaussian software with B3LYP method using a basis set 6-31g and the energy minimised structure shown at the inset in Figure 1. The higher negative value of binding energy of (-5.04 Kcal) confirms the stability of the formed adduct EDOT-PDPSA. Results showed that the adduct was formed by the charge transfer interaction between thioether group of EDOT and sulfonic acid group of PDPSA. Formation of the adduct was confirmed by measuring shift in the characteristic bands of EDOT and PDPSA in EDOT-PDPSA in the FTIR spectra. The band corresponding to the O-H stretching frequency of PDPSA observed at 3439 cm^{-1} and is shifted to 3286 cm^{-1} in EDOT-PDPSA what confirms the inter-molecular hydrogen bonding and ion-dipole interaction in EDOT-PDPSA. PDPSA exhibited peak at 1228 cm^{-1} attributed to C-O vibration which is shifted to 1224 cm^{-1} in EDOT–PDPSA revealing the extensive interaction between lone pair of electrons on -CO with EDOT. The characteristic asym(C=C) stretching peak of EDOT observed at 1460 cm^{-1} is shifted to 1459 cm^{-1} in EDOT-PDPSA. The characteristic peak of C-S observed at 976 cm^{-1} in EDOT is shifted to 876 cm^{-1} in EDOT-PDPSA. These shifts in the wave number of characteristic peaks of EDOT and PDPSA in the EDOT-PDPSA suggested the presence of various types of molecular interactions between these two molecules during the formation of the adduct.

The CMC and liquid crystalline phase formation of the self-assembled adduct "EDOT-PDPSA" was studied both in water and ethanol-water media by mixing EDOT and PDPSA in equimolar ratio. The critical micelle concentration of the EDOT-PDPSA in water and water-ethanol mixtures were determined using UV-Vis absorption measurements as 1×10^{-3} M and 5×10^{-3} M respectively.

Polarized light microscopy (PLM) is a very useful technique for the characterization of LC phase since it is possible to observe mesophases with distinct bands as a function of "EDOT-PDPSA" concentration. The PLM image showing the formation of birefringent micelles of complex shapes of disc, rod and sphere are shown Fig.2a.

Sample	Conditions solvent/T	Particle size (nm)	Conductivity (S/cm)	Mol.wt Da
PEDOTS 1	Et -H_2O / 20 ˚C	48	2.92×10^{-1}	50,000
PEDOTS 2	Et - H_2O / 60 ˚C	69	2.79	55,000
PEDOTS 3	H_2O / 20 ˚C	80	1.69×10^{-1}	40,000
PEDOTS 4	H_2O/ 60 ˚C	100	1.35	45,000
PEDOT	H_2O/ 20 ˚C	300	3.5×10^{-5}	30,000

Table 1. Properties of PEDOT nanostructures prepared in the presence and absence of PDPSA.

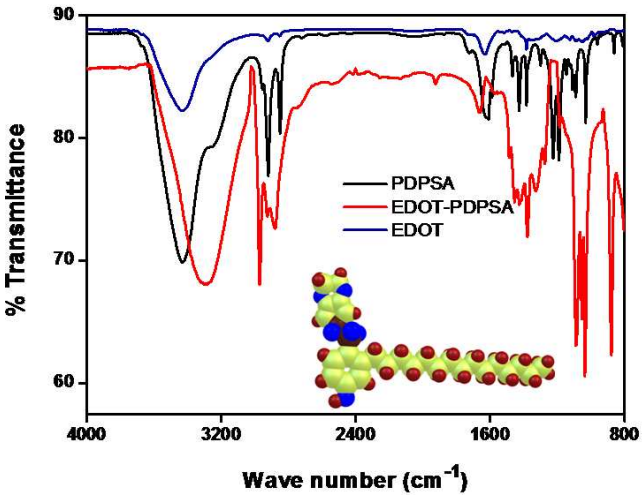

Fig 1. FTIR spectra of EDOT, PDPSA and EDOT-PDPSA.

The richness of structures with various shapes of micelle results from the weak ordering attributed to the various noncovalent interactions between EDOT-PPSA and water through self-assembly process.[26] Internal energy of this micelle is important as it enables transitions between shapes with different degrees of order. It was theoretically predicted that the intensity of inter-micellar attraction decreases in the sequence disc > rod >sphere.[26] Normally aqueous suspensions containing surfactants exhibited strictly spherical shape of micelle corresponds to a minimum in size (Shown in Figure S2). As micelles grow beyond a certain aggregation number, they forced to turn into some kind of non-spherical shape to avoid hole formation at the micellar core.[27] Under conditions of spatial confinement in a cavity, surface and bulk elastic properties compete to minimize the overall free energy [28, 29] An elastic membrane may form on the surface of the micelle by the crystallization of micelle via surface freezing to form 2D discs. When the medium of EDOT-PDPSA is changed into ethanol/water mixture, the mode of crystallization of the micelles from the surface to the centre changes and form layered structure inside the disc. Magnus et al.[30] experimentally and theoretically demonstrated that charged surfactant layers may grow both with respect to length and width to form disc like micelle and eventually the shape of the disks could become biconcave through bending elasticity and take the shape of thermodynamically stable spindle with layers inside. This is supported by the work reported by Andres F. Mejia et al.[31] At higher concentration (5×10^{-2} M); lamellar phase with micro spindle morphology has been identified under PLM. Typical PLM photograph showing the formation of microspindle shaped phase in ethanol/water are given in Fig. 2b. At higher concentration (~0.1 M) EDOT-PDPSA formed gel phase which appeared as fractograph under PLM. Typical image of the same is shown in Fig. 2c. Fig. 2d shows the formation of lamellar smectic phase in water. Different phases were formed due to the self-organization of the interdigitated bilayers of EDOT-PDPSA through various noncovalent interactions as shown in the Scheme 1 and are supported by XRD and rheological analysis which is described in the later part of the discussion.

Further Formation of liquid crystalline phase was confirmed by rheological measurements of both EDOT-PDPSA solutions under oscillatory and rotator mode. In oscillatory mode keeping constant strain (1%) elastic and viscous moduli were measured under angular frequency sweep (Fig. 3i). It can be observed that elastic modulus (G') dominates over viscous modulus (G") and maintains a constant value over a large frequency spectrum. Since a low frequency crossover is not observed in the frequency range considered and it exhibited a saddle like increase in modulus at higher frequency indicates the occurrence of dissipation mechanisms. The structure of lamellar liquid crystal phase is built from one by one bimolecular leaflets. During the action of outside force (higher frequency), they can slide between the bilayers into the flowing state in a similar manner showing plastic fluid like behavior. These two findings in the rheogram together suggest the presence of lamellar phase. This is supported by the observation made by Montalvo et. al.[29] In rotatory mode shear rate dependent viscosity measurements were made and the diagram showing the change in viscosity under varying shear rate from 300 to 1000 s^{-1} for isotropic and liquid crystalline phase (EDOT-PDPSA in water) is given in Fig. 3ii. Isotropic system showed Newtonian behavior where as the viscosity profile of LC system exhibited the non-Newtonian variation with large shear thinning behavior at lower shear rate. Secondly, the magnitude of the viscosity in liquid crystalline phase measured to be remarkably larger than Isotropic system (1238.4 Pa.S and 43.9 Pa.S). Later, on increasing the shear rate, it exhibited a relaxation type behavior similar to viscosity dependence

typically observed in smectogenic fluids as reported by Larson et al. [32]

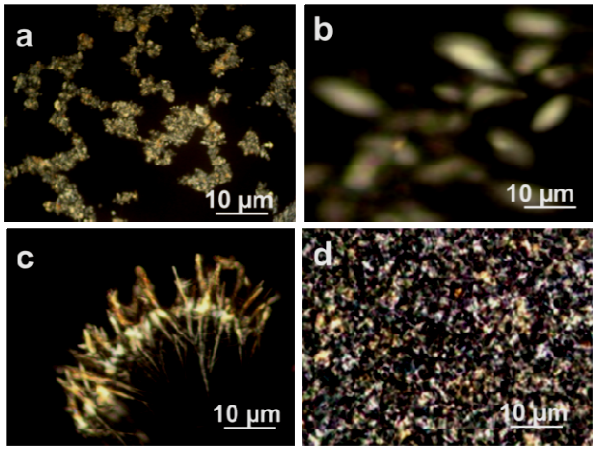

Fig 2. PLM images of EDOT-PDPSA showing the formation of (a) micelles in water, (b) spindle shaped LC phase in ethanol-water, (c) gel phase in ethanol-water and (d) hexagonal lamellar phase in water.

3.2. Synthesis of PEDOT-PDPSA by oxidative polymerization

Oxidative polymerization of liquid crystalline template 'EDOT-PDPSA' was conducted in presence of ferric chloride as the initiator. A series of color change effects were observed subsequent to the addition of initiator, $FeCl_3.6H_2O$. During the propagation process, color changes from brown to blue, green and finally to violet owing to the progress of the oxidation–reduction process leading to high molecular weight PEDOTS as shown in the Scheme1. The change of the color is attributed to the variation in the electronic state of the PEDOT and the irregularity in the nature of aggregation. Polymerization process was driven by the intrinsic properties of the self-organized lamellar phase of "EDOT-PDPSA" which act as soft anisotropic template and drives the shape and size of the formed PEDOTS. The self-assembly of EDOT-PDPSA through bilayer interdigitation forming micelles, its transformation into liquid crystalline phase and its action as soft template for the generation of PEDOTS nanospindles is illustrated in Scheme 1.

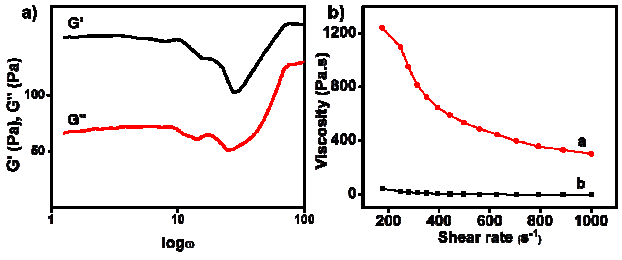

Fig 3. a) Viscoelastic properties of EDOT-PDPSA in the liquid crystalline phase as a function of Angular frequency. G' and G'' represents elastic and viscous moduli, respectively. **b)** Viscosity as a function of shear rate (a) liquid crystalline phase and (b) isotropic phase.

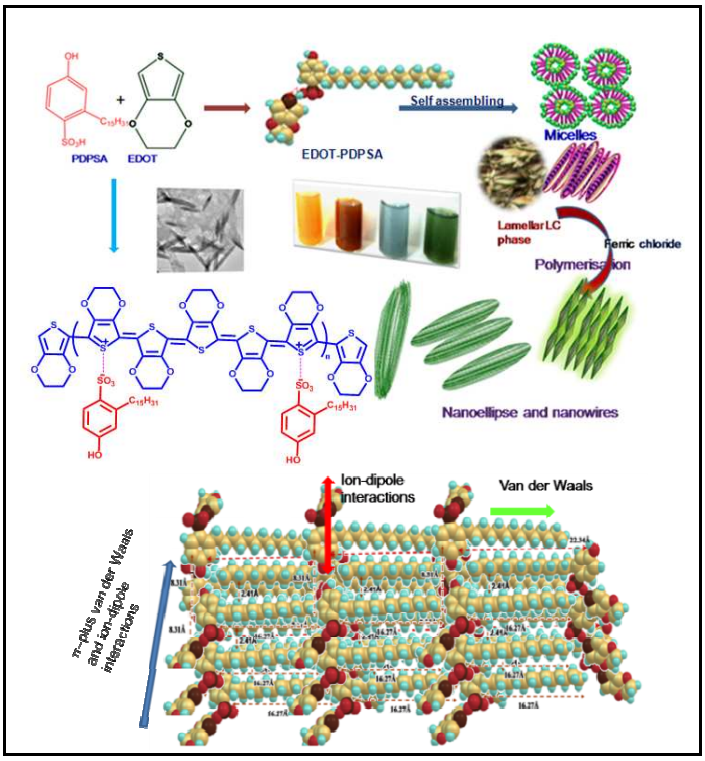

Scheme 1. Formation nanospindles of PEDOT through various steps: formation of EDOT-PDPSA adducts → micelle formation → LC phase → polymerisation to form nanospindles (top). Various noncovalent interactions present in EDOT-PDPSA to form self-organized EDOT-PDPSA through various noncovalent interactions such as alkyl chain interdigitation, π-π stacking ion-dipole interaction (bottom).

PEDOTS particles were observed to be highly dispersible in water. Particle size and polydispersity index measurement of the PEDOT dispersions were carried out using DLS technique and details are given in Table 1. Results showed that the particle size of the prepared PEDOTS nanospindles varied with change of experimental conditions. Particle size of PEDOTS1 was measured to be in the range of ~ 48 nm with polydispersity index of 0.3-0.2. However, when the polymerization temperature was increased to 60 ˚C, particle size raised to ~69 nm. Increase in temperature may accelerate the aggregation behavior, which in turn enhanced the particle size. This observation was further strengthened during molecular weight determination and morphological analysis. Particle size of PEDOTS3 observed to be ~ 80 nm at room temperature and ~ 100 nm at 60 ˚C (PEDOTS4). Particle sizes of polymer nanostructures are affected by the solvent used for their preparation.[33, 34] In ethanol-water mixture EDOT-PDPSA adopts spindle type micellar assembly which retains its shape on polymerisation and has a size of ~48 nm. But in water, due to increased polarity EDOT-PDPSA impulsively associates to form 2D ordered lamellar self-assembly. Growth of polymeric chains from lamellar self assembly in polar medium leads to aggregation of polymeric nanostructures with an approximate

size of 80 nm. PEDOT prepared in the absence of template exhibited particle size of ~ 300 nm. Molecular weight of PEDOTS was measured using MALDI TOF and found to be in the ~50,000 Da, ~ 55,000 Da, ~ 40,000Da, ~ 45,000Da, and ~ 30,000 Da with narrow molecular weight distribution for PEDOTS1, PEDOTS2, PEDOTS3, PEDOTS4 and PEDOT, respectively.

The chemical and electronic structures of the PEDOTSs were confirmed by FT-IR and UV-Vis spectroscopy. FTIR spectrum of PEDOT and PEDOTS1 is shown in Fig. 4i (a -b). PEDOT showed band at 1380 cm^{-1} which can be ascribed to the quinoid C–C structure in the thiophene ring. The band observed at 1205 cm^{-1} can be assigned to the C–O–C bond stretching, and the band corresponds to the C–S bond vibrations in the thiophene ring were found at 1004 and 750 cm^{-1}. The band observed at 1054 $cm^{-1}$is associated with the stretching vibrations in the ethylenedioxy group. The band at 1629 cm^{-1} can be attributed to the doped level of PEDOT. The bands at 2850-2980 $cm^{-1}$are associated with the characteristic -CH_2- stretching of ethylenedioxy bridge. The chemical structure of the formed PEDOTS1 exhibited similar peaks that of PEDOT with additional bands at 1305,1195 cm^{-1} due to the presence of (-SO) and the band at 1032, 574 cm^{-1} attributed to (-SO_3). All these results are consistent with the reports made by other researchers.[35-36]

UV-Vis absorption spectroscopy is a very sensitive tool for studying the nature of protonation in conducting polymers and showed obvious difference between the conducting and non-conducting state of the polymer.[37-38]The UV- Vis spectra of PEDOT, PEDOTS-1, PEDOTS-2, PEDOTS-3, and PEDOTS-4 are shown in Figure 4ii(a-e), respectively. PEDOT, PEDOTS1 and PEDOTS3 showed absorption maxima at 420 nm which can be ascribed to the π-π* electronic transition of the thiophene units. However, PEDOTS2 and PEDOTS4 showed a red shift to 480 nm showing high level of doping at high temperature. PEDOTS1 and PEDOTS3 exhibited a broad absorption band at about 800-900 nm, a feature typically seen in the doped state of conducting polymers and the absorption band at wavelength greater than this band is referred to as a "free carrier tail." This tail observed in conducting polymers with highly delocalized bipolarons. Intensity of this tail in this region in PEDOTS2 and PEDOTS4 was observed to be higher revealing the formation of more number of bipolarons at high temperature. These observations are supported by the measured high conductivity of the PEDOTS2 and PEDOTS4.

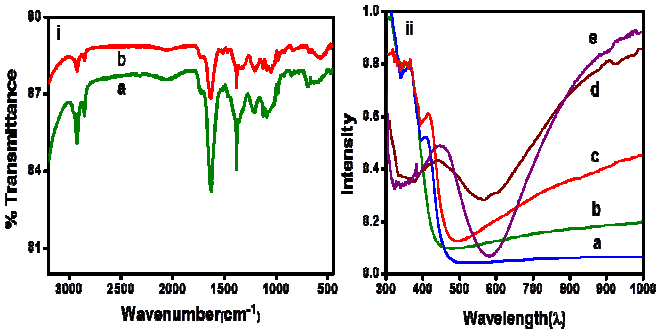

Fig 4. i) FT-IR spectrum of (a) PEDOT (b) PEDOTS and ii)UV- Vis spectra of a) PEDOT, b) PEDOTS1, c) PEDOTS3, d) PEDOTS2 and e) PEDOTS4.

3.3. XRD measurements

The nature of solid state ordering in PDPSA, liquid crystalline phase of EDOT-PDPSA, PEDOT and PEDOTS prepared under different conditions were studied by X-ray diffraction technique and are shown in Fig. 5a to 5f, respectively. PDPSA exhibited well-ordered sharp peaks with high intensity at 2θ = 2.3˚, 4.6˚ and 7.1˚ revealing the presence of high degree of crystalline order attributing from the intermolecular hydrogen bonding between the -OH and –SO_3H and also due to the ordering arising from the interdigitation of the hydrophobic layer stacking. The highest peak observed at 2θ = 2.3˚with d-spacing 36.2Å corresponds to the dimension of the self-assembled bilayered PDPSA molecule (Fig. 5a). XRD pattern of "EDOT-PDPSA" in the lamellar phase given as Fig. 5b which showed sharp peak at 2θ = 2.75˚ (32.1Å) and a broad peak 2θ =3.62˚ (24.38Å) revealing the presence of supramolecular organization with liquid crystalline hexagonal phase. It also exhibited sharp peaks at 2θ = 5.08˚ (17.37Å), 2θ = 9.67˚ (9.13Å) and 2θ = 12.00˚ (7.37Å). The peak observed at 2θ = 23.83˚corresponds to the d-spacing of 3.73Å corresponds to the inter-planar distance of the adjacent ethylene dioxythiophene centres. The observed d-spacing in "EDOT-PDPSA" was found in good correlation with the dimensions of the optimized interdigitated structure of EDOT-PDPSA obtained from Gaussian software with B3LYP method using a basis set of 6-31g (Fig. 5 given inset). It showed head to tail distance of EDOT-PDPSA ~22.34 Å, distance between the interdigitated alkyl chains~2.4 Å, length of the extended hydrophobic chain~16.27 Å, and the distance between the interdigitated thiophene head groups ~ 8.31 Å.

All PEDOTSs exhibited high intense peak at 2θ = 2.8-3.5˚ with average d-spacing ~26.36 Å corresponding to the dimension of the self-assembled supramolecular PEDOTS structures. XRD pattern of PEDOTSs prepared from both water and ethanol-water at 20 ˚C showed peak at 2θ = ~3.35˚ (26.34 Å). But for PEDOTS2 it is shifted to 3.26˚ with d-spacing of 27.07Å revealing higher dimension for the aggregated self-assemblies. PEDOTS3 exhibited this signal at 2θ = 2.82˚ with a d-spacing of 31.29Å. The diffraction peak at 2θ = 25.5˚ (d-spacing 3.5 Å)

corresponds to the inter-planar ring stacking distance. However, it was noted that XRD pattern of PEDOTs prepared in water exhibited weak broad peaks, compared with the batches prepared in ethanol-water mixture which suggest less ordering for PEDOTS prepared from aqueous medium. However, PEDOTS3 (Fig. 5d) prepared at higher temperature showed peak at 2θ = 25.5°with a higher d-spacing suggesting a loose molecular interaction between the stacked ring and larger size for stacking aggregates. Here inclusion of the dopant ion pulls polymeric chains apart making necessary room for solvent inclusion. These will facilitate more water molecules to intrude the polymeric matrix, making it more water dispersible. PEDOT prepared in the absence of PDPSA showed broad weak signal between 2θ= 19-25°revealing amorphous nature.

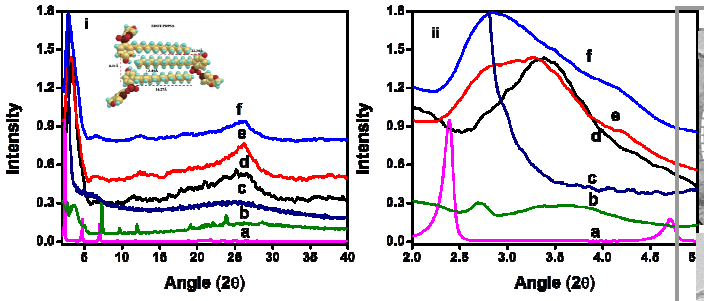

Fig 5. i) Powder XRD patterns of a) PDPSA, b) EDOT-PDPSA, c) PEDOT, d) PEDOTS2, e) PEDOTS1 and f) PEDOTS3. Energy minimized double layer geometry of EDOT-PDPSA is given in inset and **ii)** magnified lower angle portion of Powder XRD.

3.4. Morphology and mechanism of PEDOT nanospindles formation

Energy minimized structure of adduct "EDOT-PDPSA" using Gaussian program suggested an extended conformation with bent structure for the "EDOT-PDPSA" indicating its propensity for the formation of self-assembled supramolecular structures through various noncovalent interactions. XRD of aggregated "EDOT-PDPSA" showed d-spacing of ~ 32.1Å which is slightly less than twice the molecular length of "EDOT-PDPSA" suggested the presence of interdigitated molecular layers in the supramolecular aggregates as shown in the scheme. At low concentration, they were observed to form micelles of various shapes, which will be randomly dispersed in the solvent and the PLM picture (Fig. 2a) showed presence of mixture of spherical and disc shaped micelles. Above critical micellar concentration, "EDOT-PDPSA" exhibited the formation of lyotropic phase. This might have formed by coalescence of various micelles and later they reorganized to form thermodynamically stable spindle shaped lamellar phase in ethanol-water and thread like hexagonal phase in water.Spindle shape of the liquid crystalline phase may be attributed to the strong intermolecular interaction among the charged ions present in the head groups and counter charge in EDOT, hydrophobic tails and also inter planar π-π stacking. The interdigitated bilayers formed by the "EDOT-PDPSA" ensembles as shown in Scheme1.

These supramolecular assemblies are thermodynamically stable and may take the shape of spindle as shown in the Fig. 2b. Lyotropic phase of "EDOT-PDPSA" in water exhibited lamellar smectic phase as shown in Fig. 2d. Morphological variation during polymerization of "EDOT-PDPSA" in ethanol-water and water were followed by taking TEM images in definite time intervals. Initially nanoscopic spindle shaped PEDOTS were observed under TEM. In the propagation step, PEDOTS aggregates which are in the lyotropic mesophase may lose molecular order on a nanometer scale due to the thermodynamic influence of the growing chain. They form thermodynamically stable spindles of inherent nanoscale dimensions via self-assembly.

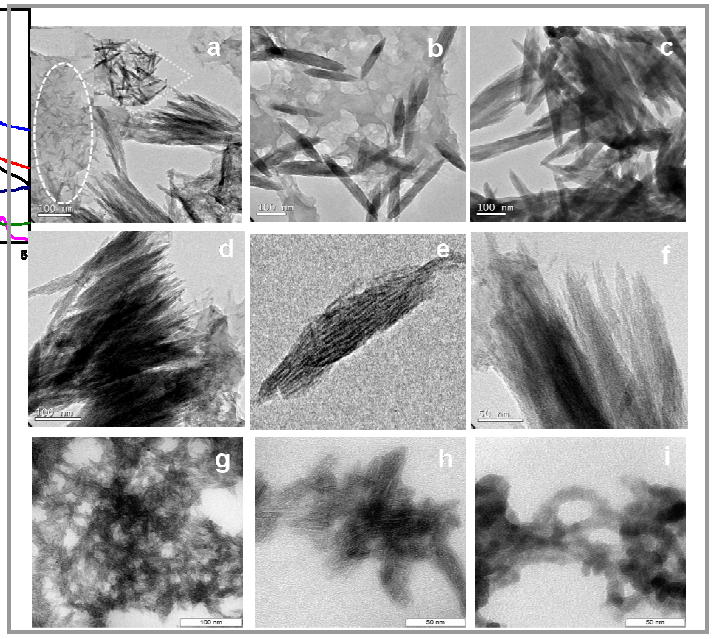

Fig. 6. Morphological evaluation of PEDOTS during the course of polymerization: a) sidewise etching of subnanospindles to nanospindles. PEDOTS1 b) after 6 hrs, c) after 12 hrs, d) after 24 hrs, e) single nanospindle showing subnanofibrils or discs, f) PEDOTS2 after 24 hrs g) PEDOTS3 h) nanofibrils of PEDOTS3 after 24 hrs, i) nanofibrils of PEDOTS4.

TEM picture showing the formation of sub-nanospindles and later aggregating to form nanospindles through side-wise etching are shown in Fig. 6a. PEDOTS1 exhibited uniform nanospindles of 20 nm width and 200 nm lengths after 6 hrs (Fig. 6b). However, when the polymerization time increased to 12 hrs, PEDOTS1 observed as slightly elongated spindles of 30 nm width and 300 nm lengths and after 24 hrs spindles of 50nm width 300nm length were observed (Fig. 6c and d). Similar observations were made by O' Brien et al.[39] They successfully prepared varieties of liquid crystalline assemblies with the preservation of the shape of the mesostructures of the

monomers. These observations were further strengthened by the studies made by Stup et al.[20] They proposed that the observed structure results from the template directed aggregation of the oriented polymer chains which preserve the shape of the liquid crystalline template.

TEM image showing a single nanospindle composed of subnanofibrils is shown in Fig. 6e. It further confirms the formation of nanospindles from micelles of lower dimensions having disc or fibrillar morphology. It has been observed at high temperature, the oriented nanofibrils confined inside the nanospindles blossoms out with fibrils of high aspect ratio due to the changes in the thermodynamic properties and the mode of molecular packing at high temperature. TEM image of PEDOTS2 synthesized at 60 ˚C showed nanowhisker/ fibrillar morphology as shown in Fig. 6f. TEM images of PEDOTS3 prepared from water dispersion at 20˚C for 6 hrs showed networks of nanofibrils as shown in Fig. 6g. However, after 24 hrs these nanofibrils transformed into a more ordered nanofibers with high aspect ratio (Fig 6h). PEDOTS4 prepared at 60 ˚C in water exhibited nanowires of 20-30 nm diameter and several orders of micrometer length attributed to the hierarchical aggregation of the self-assembled nanofibrils as shown in Fig. 6i. SEM analyses of PEDOTS also confirm the formation of nanofibrils and nanowires (Fig. S3a-S3c). SEM image of PEDOT prepared in the absence of PDPSA showed no specific morphology (Fig. S3d) revealing the contribution of PDPSA in the formation of template. SAED patterns showing the presence of well-ordered nanospindles and nanowires are given in the supporting information as Fig. S4a and S4c. Our observation is contrary to the reports made by Mao et. al.[22] They prepared PEDOT nanospindles using $FeCl_3$ as initiator in presence of CTAB and PAA as template. They reported that the observed nanospindles are attributed to the co-crystallization of PEDOT and β-akagenite and they observed its characteristic crystalline peaks in XRD and the stoichiometric amount of iron in EDAX spectra. However, we could neither observe the characteristic crystalline peaks of β-akagenite in XRD nor stoichiometric amount of iron in EDAX confirming the spindle formation is ascribed exclusively to the imitation of liquid crystalline template and not by the simultaneous occurrence of polymerization of EDOT and crystallisation of Fe^{3+}. Nevertheless, EDAX of PEDOTS1 prepared from ethanol-water showed the presence of some amount of iron, which may be contributed from the free iron hydroxide retained during the purification step. Typical EDAX profile of PEDOT nanospindles and nanowires are given in the ESI (Fig. S4b and S4d). The size of the nanospindles and nanofibrils could be adjusted by controlling the reaction conditions.

3.5.. Conductivity studies and thermal stability

DC conductivity of pelletized samples of PEDOTS was measured using Four-probe conductivity meter. Details regarding the composition and conductivity are depicted in Table 1. Conductivities of PEDOTSs prepared under different experimental condition showed significant variation. PEDOT prepared in the absence of template exhibited conductivity in the order of 3.5×10^{-5} S/cm. However, PEDOTS1, PEDOTS2, PEDOTS3 and PEDOTS4 have conductivity of 2.96×10^{-1} S/cm, 2.79 S/cm, 1.69×10^{-1} S/cm and 1.35 S/cm respectively. Sulphonate ions acts as smooth relay bridges in between the polymeric chains for charge carriers and thereby enhancing the conductivity in a significant manner. In a recent report, PEDOT: PSS films prepared by template method exhibited conductivity of 2 S/cm which is less than that of PEDOTS.[40] This also supports the utility of PEDOTS in photovoltaic devices as charge transport layer. Any nano formulations with pointed ends are capable of accumulating charges and transfer to other parts. T. P. Lodge et al showed that their nano porous PEDOT fibrous film has a conductivity of 5.4×10^{-4} S/cm which is comparatively lower than that of PEDOT hexagonal rods prepared by Remita et. al (0.4 S/cm).[41,42] Kim et al reported PEDOT nano fibers with a higher conductivity of 1 S/cm.[43] M. H. Lee et al reported PEDOT/PSSA spherical nano particles with a conductivity of 0.11 S/cm.[44] These observations suggest that bulk aggregated films have lower conductivity in comparison with distinctly separated nano structures. Also, elongated nano structures with tapered ends have more conductivity than spherical particles. In our case we got a maximum conductivity of 2.79 S/cm due to the nanospindle morphology. Nano spindles with pointed ends facilitate smooth transfer of charge carriers resulting in higher conductivities which can be applied in different fields as anisotropic conductors. It may also find place by replacing PEDOT/PSS as charge carrier for various energy devices. Further, a comparative study showing the effect of shape on the electrical conductivity PEDOT nanoparticles is illustrated in Table S1.

Conducting polymers with good conductivity and thermal stability are desirable for the high energy applications.[45] Thermal stability studies were carried out in DTG analyzer under nitrogen atmosphere. PEDOTS1, PEDOTS3 and PEDOT were observed to be decomposing at 310 ˚C, 315˚C and 290˚C with char yield of 6.9 %, 6.5% and 4.1%, respectively. The higher thermal stability exhibited by PEDOTS compared with PEDOT may be due to the high molecular weight and also due to the presence of doped ions. Thermograms of PEDOTS1, PEDOT3 and PEDOT are shown in Fig. S5a to S5c, respectively in ESI.

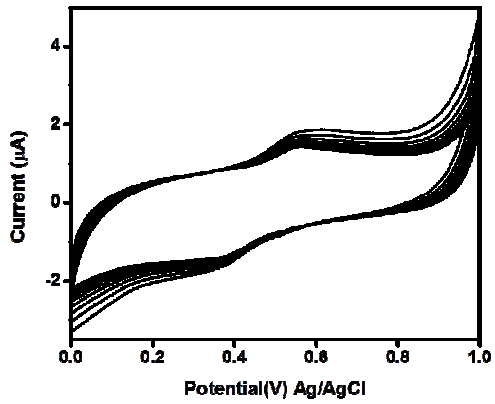

Fig. 7. Cyclic voltammogram of PEDOTS3 in 0.1M H_2SO_4. Scan rate 0.05 V/sec.

3.6. Electrochemical behavior and CV responses of L-ascorbic acid using nanospindle PEDOT modified GCE

The electrochemical behavior of PEDOTS was studied by cyclic voltammetry (CV). CV response of PEDOTS1 modified GCE in 0.1 M H_2SO_4 with scanning rate 0.05 V/s is showed in Fig. 7. It exhibited weak redox peaks at 0.562V (oxidation) and 0.37V (reduction) referred to a standard Ag/AgCl electrode, which is characteristic feature of PEDOT.

Experiments were performed for studying the electro catalytic activity of modified GCE with PEDOTS on the oxidation of ascorbic acid. Fig. 8(i) shows the cyclic voltammograms of the PEDOTS modified GCE and bare GCE in phosphate buffer solution (PBS) (pH = 7.4 at 27 °C with a scanning rate of 0.05V/s). Bare GCE did not give any CV response (Fig. 8ib) and current obtained is much lower than the modified GCE (Fig. 8ia). The CV measurements have been carried out in PBS with 1 mM L- ascorbic acid. The oxidation potential of L-ascorbic acid appeared around at 0.357V with a peak current of 4.7μA. It was found that the oxidation peak was broad and no peak in the reverse scan was observed, which indicated that the oxidation of ascorbic acid at the bare electrode is totally irreversible (Fig. 8 iib). However, the CV diagram of PEDOTS modified GCE showed the oxidation peak of ascorbic acid at 0.046 V compared to the bare GCE, the peak current was about 10 times (91.68 μ A) higher than that of the bare GCE, which revealed the electro-catalytic oxidation of ascorbic acid at the modified GCE(Fig. 8 iia). This is supported by the work done by other researchers.[46] According to literature, the large cathodic shift in the oxidation potential and the enhanced oxidation current may be due to the electrostatic attractions between the cationic charged PEDOTS backbone on the modified GCE and the ascorbate anions in the solution. Also from the FTIR data, it is evident that the doped PEDOT contains sulphonate anions, which could be partly exchanged by the ascorbate anions and might accumulate at the interface of the modified GCE. Fig 8 iii shows the CV responses of the modified GCE in PBS with different concentrations of L-ascorbic acid. The effect of scanning rate and the CV responses of the electro-catalytic oxidation of ascorbic acid using modified GCE is shown in Fig. 8 iv. It was found that the nature of the oxidation process in PBS proceeds by diffusion control as evidenced from the plots of square root of scan rate vs. peak current. Their good linear dependence and the low detection limit showed significant sensitivity of PEDOTS nanospindles modified GCE for the detection of ascorbic acid in aqueous solutions.

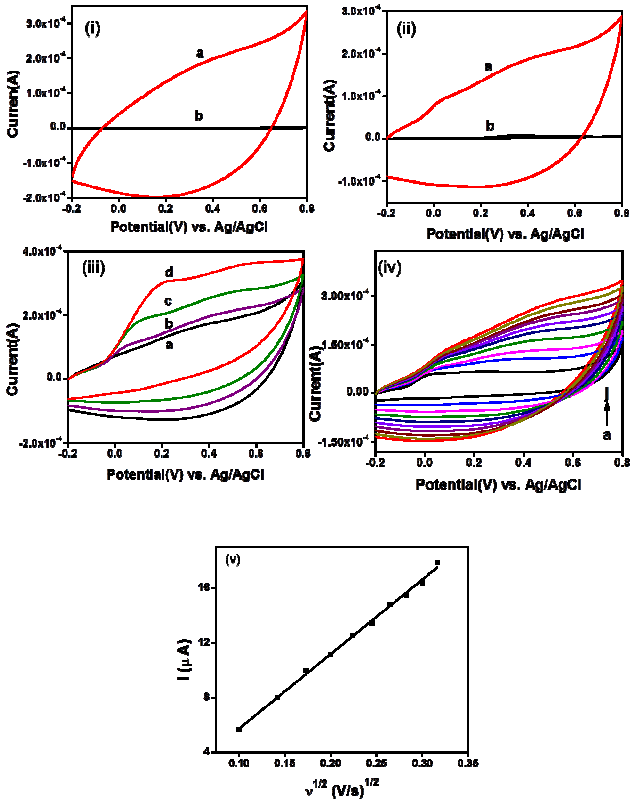

Fig. 8. Cyclic voltammetric responses in the presence and absence of L-ascorbic acid (AA) in PBS buffer (pH=7.4) **i)** without AA a) PEDOTS modified electrode and b) bare GCE. **ii)** In presence x10^{-3} M AA a) PEDOTS modified electrode and b) bare GCE. **iii**) Effect of AA concentration on CV responses of modified electrode in PBS buffer a) 5x10^{-5} M b)10^{-4} M c)10^{-3} M and d) 5x10^{-3}M AA **iv**) Effect of scan rate on the cyclic voltammetric responses of PEDOTS nanospindles modified GCE (a) 10; (b) 20;(c) 30; (d) 40; (e) 50; (f) 60; (g) 70; (h) 80; (i) 90; (j) 100 mV/s in PBS with 1 mM L-AA. **v**) Plot of square root of scan rate vs. peak current.

Conclusions

Water dispersible nanospindles of PEDOTS with controlled size, shape and microstructure were prepared using polymerization of the liquid crystalline template EDOT-PDPSA. It was observed that morphology of PEDOT could be tuned from nanofibrils to nanospindles and wires by controlling

the experimental conditions. Solid state ordering in template monomer and polymer was confirmed by XRD and SAED pattern. The formation of nanospindles and nano whiskers were confirmed by SEM and TEM. Nano spindles of conducting PEDOTs with pointed ends pose a suitable candidate for charge transfer in nanoelectronic devices. Studies on the electrochemical stability and electro catalytic activity of PEDOT nanospindles modified GCE suggests its application for the electrocatalytic oxidation of ascorbic acid and similar molecules. Electrical conductivity of PEDOTS observed as ~2.79 S/cm and its high thermal stability of ~300˚C suggest that, these water dispersible nanomaterials can be used as hole transport layer in photovoltaics.

Acknowledgements

We thank CSIR and UGC for the financial support. We also would thank Dr. Suresh Das, Director, NIIST, TVM for the constant encouragement and support. We are also thankful to P. Guruswamy, M. Chandran, Mrs. L. Paul and K. Mohan for XRD, SEM and TEM analysis. We are also thankful to the finanace support from CSIR network projects TAPSUN (NWP-54) and MULTIFUN(CSC0101) and ISRO (GAP 133839)

Notes and references

[a] Address here.

[b] Address here.

[c] Address here.

† Footnotes should appear here. These might include comments relevant to but not central to the matter under discussion, limited experimental and spectral data, and crystallographic data.

Electronic Supplementary Information (ESI) available: [Materials and methods, CMC determination, PLM and SEM images]. See DOI: 10.1039/b000000x/

References

1. T.A. Skotheim, R. L. Elsenbaumer and J. R. Reynolds, *Handbook of Conducting Polymers, Second Edition*, Marcel Dekker, Newyork, 2 edn., 1997.
2. H. S. Nalwa, *Handbook of Organic Conductive Molecules and Polymers: Conductive polymers : transport, photophysics, and applications*, Wiley,Chichester, 1997.
3. A. J. Heeger, *J. Phys. Chem. B*, 2001, **105**, 8475-8491.
4. A. G. MacDiarmid, *Angew. Chem. Int. Ed.*, 2001, **40**, 2581-2590.
5. H. Xie, S.-C. Luo and H.-h. Yu, *Small*, 2009, **5**, 2611-2617.
6. K. C. See, J. P. Feser, C. E. Chen, A. Majumdar, J. J. Urban and R. A. Segalman, *Nano Lett.*, 2010, **10**, 4664-4667.
7. W. Gaynor, G. F. Burkhard, M. D. McGehee and P. Peumans, *Adv.Mater.*, 2011, **23**, 2905-2910.
8. R. Liu, J. Duay and S. B. Lee, *ACS Nano*, 2010, **4**, 4299-4307.
9. L. Groenendaal, F. Jonas, D. Freitag, H. Pielartzik and J. R. Reynolds, *Adv. Mater.*, 2000, **12**, 481-494.
10. F. A. Boroumand, P. W. Fry and D. G. Lidzey, *Nano Lett.*, 2004, **5**, 67-71.
11. F.-C. Tang, J. Chang, F.-C. Wu, H.-L. Cheng, S. L.-C. Hsu, J.-S. Chen and W.-Y. Chou, *J. Mater. Chem.*, 2012, **22**, 22409-22417.
12. V. Rumbau, J. A. Pomposo, A. Eleta, J. Rodriguez, H. Grande, D. Mecerreyes and E. Ochoteco, *Biomacromolecules*, 2007, **8**, 315-317.
13. F. C. Krebs, *Org. Electron.*, 2009, **10**, 761-768.
14. S. Chen, Y. Li and Y. Li, *Polym. Chem.,* 2013, **4**, 5162-5180.
15. Y.-Z. Long, M.-M. Li, C. Gu, M. Wan, J.-L. Duvail, Z. Liu and Z. Fan, *Prog. Polym. Sci.*, 2011, **36**, 1415-1442.
16. M. G. Han and S. H. Foulger, *Small*, 2006, **2**, 1164-1169.
17. A. Gök, M. Omastová and A. G. Yavuz, *Syn. Met.*, 2007, **157**, 23-29.
18. V. Tsakova, S. Winkels and J. W. Schultze, *Electrochimi. Acta*, 2001, **46**, 759-768.
19. S. S. Babu, V. K. Praveen, and A. Ajayaghosh, *Chem. Rev*., 2014, **114**, 1973–2129.
20. J. F. Hulvat and S. I. Stupp, *Angewa. Chem. Inte. Ed.*, 2003, **42**, 778-781.
21. J. Hain, M. Schrinner, Y. Lu and A. Pich, *Small*, 2008, **4**, 2016-2024.
22. H. Mao, X. Lu, D. Chao, L. Cui, Y. Li and W. Zhang, *J. Phy. Chem. C*, 2008, **112**, 20469-20480.
23. J. D. Sudha, S. Sivakala, C. K. Chandrakanth, K. S. Neethu, K. N. Rohini and R. Ramakrishnan, *eXPRESS Polym. Lett..,* 2014, **8**,107–115.
24. J. D. Sudha and S. Sivakala, *Colloid Polym. Sci.,* 2009, **287**, 1347-1354.
25. J. D. Sudha, V. L. Reena and C. Pavithran, *J.Polym.Sci.Part B: Polym.Phys.*, 2007, **45**, 2664-2673.
26 J. Zhang, X.-F. Chen, H.-B. Wei and X.-H. Wan, *Chem.Soc.Rev.*, 2013, **42**, 9127-9154.
27. S. V. Burylov, *J. Exp. Theor. Phys*., 1997, **85**, 873-886.
28. T. Zemb, M. Dubios, B. Deme and T. G.-Kryzywicki, *Science*, 1999, **283**, 816–819.
29. G. Montalvo, M. Valiente and E. Rodenas, *Langmuir*, 1996, **12**, 5202-5208.
30. M. Bergström, *Langmuir*, 2006, **22**, 6796-6813.
31. A. F. Mejia, P. He, M. Netemeyer, D. Luo, M. Marquez and Z. Cheng, *Soft matter*, 2010, **6**, 4885-4894.
32. R. G. Larson, *The Structure and Rheology of Complex Fluids*, Oxford, University Press, New York, 1999.
33. J. H. Fendler, *Chem. Rev*., 1987, **87**, 877-899.
34. S. R. Saunders, M. R. Eden, and C. B. Roberts, *J. Phys. Chem. C*, 2011, **115**, 4603–4610.
35. J. W. Choi, M. G. Han, S. Y. Kim, S. G. Oh and S. S. Im, *Syn. Met.*, 2004, **141**, 293-299.
36. H. J. Ahonen, J. Lukkari and J. Kankare, *Macromolecules*, 2000, **33**, 6787-6793.
37. D. Hohnholz, A. G. MacDiarmid, D. M. Sarno and J. W. E. Jones, *Chem. Commun.*, 2001, 2444-2445.
38. R. Corradi and S. P. Armes, *Syn. Met.*, 1997, **84**, 453-454. 32.
39. M. K. Fung, S. L. Lai, S. W. Tong, M. Y. Chan, C. S. Lee, S. T. Lee, W. W. Wu, M. Inbasekaran and J. J. O'Brien, *Appl. Phys. Lett.*, 2002, **81**, 1497-1499.
40. S. Timpanaro, M. Kemerink, F.J. Touwslager, M.M. De Kok and S. Schrader, *Chem. Phys. Lett*., 2004, **394**, 339-343.
41. B H. Jones, K.-Y. Cheng, R. J. Holmes and T. P. Lodge, *Macromolecules,* 2012, **45**, 599−601.

42. S. Ghosh, H. Remita, L. Ramos, A. Dazzi, A. D.-Besseau, P. Beaunier, F. Goubard, P.-H. Aubert, F. Brissetf and S. Remita, *New J. Chem*., 2014, **38**, 1106-1115.
43. S. Nair, E. Hsiao, and S. H. Kim, *Chem. Mater*., 2009, **21**, 115–121.
44. H. S. Kang, S.-Y. Park, K. Kim, J.-W. Kim, H. Jeong, S. H. Lee and M.-H. Lee, *Macromol. Res*., 2013, **21**, 693-698.
45. C.-H. Chiang and C.-G. Wu, *Org. Electron.*, 2013, **14**, 1769-1776.
46. S. S. Kumar, J. Mathiyarasu, K. L. N. Phani and V. Yegnaraman, *J Solid State Electrochem.*, 2006, **10**, 905-913.

TOC